Mesoscale Predictability of Moist Baroclinic Waves: Experiments with Parameterized Convection

ZHE-MIN TAN

Department of Atmospheric Sciences, Nanjing University, Nanjing, China

FUQING ZHANG

Department of Atmospheric Sciences, Texas A&M University, College Station, Texas

RICHARD ROTUNNO AND CHRIS SNYDER

National Center for Atmospheric Research, Boulder, Colorado*

(Manuscript received 7 May 2003, in final form 22 January 2004)

ABSTRACT

Recent papers by the authors demonstrated the possible influence of initial errors of small amplitude and scale on the numerical prediction of the ''surprise'' snowstorm of 24–25 January 2000. They found that initial errors grew rapidly at scales below 200 km, and that the rapid error growth was dependent on moist processes. In an attempt to generalize these results from a single case study, the present paper studies the error growth in an idealized baroclinic wave amplifying in a conditionally unstable atmosphere. The present results show that without the effects of moisture, there is little error growth in the short-term (0–36 h) forecast error (starting from random noise), even though the basic jet used here produces a rapidly growing synoptic-scale disturbance. With the effect of moisture included, the error is characterized by upscale growth, basically as found by the authors in their study of the numerical prediction of the surprise snowstorm.

1. Introduction

Lorenz (1969) hypothesized that even if forecast errors were to be reduced through improvements in either the forecast models or their initial conditions, errors due to small-scale motions may grow in amplitude and scale so rapidly that they place an effective limit on the predictive skill of a model. Recent papers by Zhang et al. (2002, hereafter ZSR02) and Zhang et al (2003, hereafter ZSR03) focusing on the ''surprise'' snowstorm of 24–25 January 2000 demonstrate the influence of initial errors of small amplitude and scale on the numerical prediction of that storm. They found that initial errors grew rapidly at scales below 200 km, and that the rapid error growth was dependent on moist processes. Here, we report on our attempt to isolate within an idealized context this error-growth behavior.

The snowstorm of 24–25 January 2000 on the southeastern coast of the United States was the result of an amplifying, eastward-moving, synoptic-scale wave (see Fig. 8 of Langland et al. 2002). Using the U.S. Navy global forecast model and (dry) adjoint system, Langland et al. (2002, see their Table 1) showed that the 3–4-day forecast for the East Coast for 1200 UTC 25 January 2000 was in considerable error, and very sensitive to the model initial condition; in comparison with the 3–4-day forecasts, the 1–2-day forecasts were considered to be moderately good from the synoptic-scale perspective, and far less sensitive to initial-condition error. Using the fifth-generation Pennsylvania State University (PSU)–National Center for Atmospheric Research (NCAR) Mesoscale Model (MM5; Dudhia 1993), ZSR02 investigated the 0–36-h forecast for the same case; MM5 forecasts initialized from several different operational initial analyses showed, consistent with Langland et al. (2002), similarly good skill from a large-scale perspective, but rather large differences among the forecasts in their mesoscale precipitation patterns.

By comparing simulations of the same case in which the initial conditions differed by a small-amplitude perturbation concentrated at the smallest resolvable scale, ZSR03 showed how the error in the 36-h forecast precipitation pattern originates in small scales and then

* The National Center for Atmospheric Research is sponsored by the National Science Foundation.

Corresponding author address: Dr. Fuqing Zhang, Department of Atmospheric Sciences, Texas A&M University, College Station, TX 77845-3150.
E-mail: fzhang@tamu.edu

amplifies as it spreads upscale and that the error growth is associated with conditional instability and (parameterized) moist convection. This is in general agreement with the results of Ehrendorfer et al. (1999), using a mesoscale model and its adjoint including moist processes; they also showed that, in the presence of parameterized moist convection, errors may grow more rapidly and at smaller scales than in a dry version of the model. In their highest-resolution experiments (inner grid of 3.3-km horizontal resolution without a parameterization of moist convection), ZSR03 found that the small-scale differences appeared first as differences in the timing and placement of convective cells and then spread upscale to alter the shape and location of the surface cyclone in the 36-h forecast.

Our focus in this paper is on the potential for initial errors of small scale and small amplitude to impose an intrinsic limit on the predictability of mesoscale flows, even in the absence of other sources of error. In practice, of course, the skill of today's weather forecast may be influenced by numerous factors, such as analysis errors of significant amplitude and synoptic scale, errors in the lateral boundary conditions and errors in the forecast model itself. For the snowstorm of 24–25 January 2000, ZSR02 showed that each of those additional factors may well have contributed to the poor operational forecast. Although the scope of the present paper will be limited to the growth of small-scale and small-amplitude initial errors, we emphasize that, as in the snowstorm of 24–25 January 2000, other sources of forecast error are possible. A discussion of these other sources and a more complete review of the literature on mesoscale predictability can be found in ZSR02 and ZSR03.

Motivated by the observation that the snowstorm of 24–25 January 2000 was associated with the downstream amplification of a synoptic-scale wave and wishing to generalize the results of ZSR02 and ZSR03 from a single case, we have carried out MM5 simulations of an idealized baroclinic jet in a channel with a prescribed initial synoptic-scale perturbation restricted to the western (upstream) end of the channel. The latter problem has been extensively studied (see Hakim 2000 for a recent review) as a model for the observed amplification of synoptic-scale waves. To the idealized baroclinic jet, we have added a moisture distribution so that the idealized atmosphere is conditionally (as well as baroclinically) unstable. This experimental setup allows us to investigate in a simpler, but still realistic, context the suggestion of ZSR03 that the rapid error growth seen in their simulations required conditional instability and either moist convection (in the highest-resolution runs) or its parameterization.

The paper is structured as follows. A brief introduction to the numerical model, initial condition and experimental design for the work are presented in section 2, followed in section 3 by a description of the simulation of the idealized moist baroclinic wave. Section 4 analyzes the error growth within that baroclinic wave. Dependence of the error growth on the waves' initial moisture distributions is explored in section 5. Section 6 contains a summary.

2. Model description, initial condition, and experimental design

a. Model description

To study the mesoscale structure within an evolving synoptic-scale wave, we employ here MM5 (version 2) on two model domains (D1, D2) with 90- and 30-km horizontal grid resolution, respectively, and 60 vertical layers. For simplicity, the model employs Cartesian coordinates and a constant Coriolis parameter. Domain D1 is configured in the shape of a channel 18 000 km long (east–west or x direction) and 8010 km wide (north–south or y direction), while D2 is a rectangular subdomain 8400 km long and 4800 km wide centered at (9720 km, 3960 km) within D1. The Grell (1993) cumulus parameterization, the MRF planetary boundary layer scheme (Hong and Pan 1996), the Reisner microphysics scheme with graupel (Reisner et al. 1998), and a simple radiation parameterization are used in both domains. At the lower boundary, a drag law (with uniform surface roughness length $= 10^{-4}$ m) and no heat/moisture flux are applied throughout the domain. In addition to its use of an idealized initial flow, the present simulation thus also neglects physiographic effects associated with orography and heat and moisture fluxes from the ocean. Although the latter certainly plays some role in coastal storms of the type that produced the snowstorm of 24–25 January 2000, their conscious neglect here eliminates a potential sensitivity and simplifies the interpretation of the results.

b. Initial condition

The initial condition of an idealized two-dimensional baroclinic jet with a balanced three-dimensional perturbation is generated through the following steps.

- *Step 1.* We first create a zonally invariant baroclinic jet by specifying the position of the tropopause as a function of y and z, with constant potential vorticity (PV) in both the troposphere [0.4 PV units (PVU), where 1 PVU $= 10^{-6}$ m^2 s^{-1} K kg^{-1}] and stratosphere (4.0 PVU), as in Rotunno et al. (1994, hereafter RSS94). The value of 1.5 PVU is used to define the location of the tropopause, which is indicated by the thick-dashed line in the y cross section of Fig. 1a. For more information on the specification of the base-state PV, refer to the appendix in RSS94.
- *Step 2.* The balanced wind and potential temperature fields for the jet, also shown in Fig. 1a, are obtained by inverting the PV in the y–z plane. A two-dimensional version of the PV inversion technique developed by Davis and Emanuel (1991) is used.
- *Step 3.* A localized, synoptic-scale, balanced pertur-

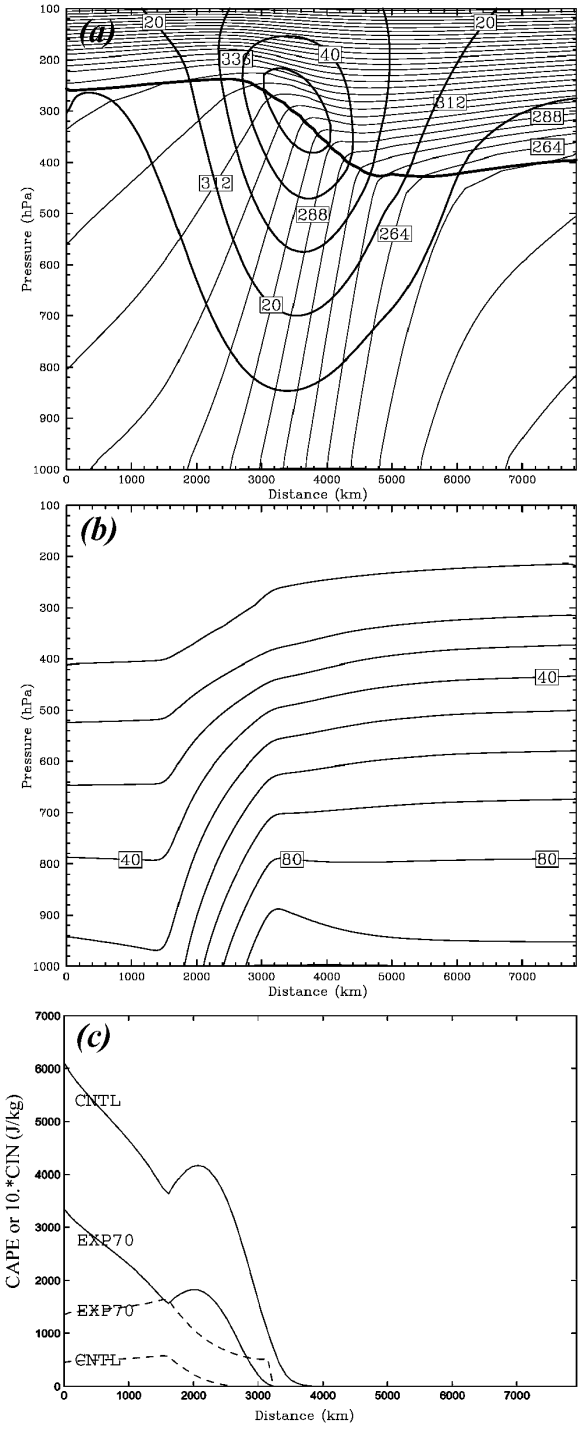

FIG. 1. (a) Vertical cross section of initial potential temperature (thin line, $\Delta = 6$ K) and zonal velocity (thick line, $\Delta = 10$ m s^{-1}) for the initial basic-state jet. The gray thick line denotes the location of the tropopause where potential vorticity equals 1.5 PVU. (b) Vertical distribution of the initial relative humidity for the control experiment ($\Delta = 10\%$). (c) Meridional variation of surface CAPE (solid) and CIN (dashed) for both the CNTL experiment and EXP70.

bation of moderate amplitude is then added to the base state from step 2 to represent the early phase of a typical midlatitude cyclogenesis. Similar to Rotunno and Bao (1996), the perturbation is obtained by specifying a horizontal displacement field, calculating a PV perturbation by multiplying that displacement by the meridional gradient of PV. For more information on the specification of the PV perturbation, refer to Rotunno and Bao (1996, p. 1057).

- *Step 4.* We then invert the 3D perturbed PV fields from step 3 to obtain the streamfunction and geopotential (and thus wind and temperature) fields again using the PV inversion technique of Davis and Emanuel (1991).
- *Step 5.* The initial relative humidity (RH) is given by (A1) in the appendix. The control experiment uses $(\mathrm{RH})_0 = 100\%$ in (A1), which yields strong conditional instability in the southern portion of the domain in the control experiment. The resulting initial distribution of RH in the control experiment varies from 100% at the lowest level to 10% above a height of 8 km and is shown in Fig. 1b. The surface convective available potential energy (CAPE) and surface convective inhibition (CIN) along the meridional cross section are shown in Fig. 1c.

The combination of the baroclinic jet and a balanced moderate-amplitude PV disturbance ensures the strong development of a baroclinic wave as discussed in Hakim (2000). The same balanced initialization method but for a dry baroclinic wave was used in Zhang (2004).

c. Experimental design

For the control experiment (CNTL), the model is integrated on the coarse domain (D1) for 72 h using the balanced initial conditions constructed as detailed above and fixed lateral boundary conditions. We envision this integration to be analogous to a global model forecasting an amplifying, eastward-propagating synoptic-scale disturbance. The inner domain (D2) of the model is initialized at 36 h by interpolating from the solution on D1. The integration on D1 then proceeds for 36 h with lateral boundary conditions provided by D1 through one-way nesting. Hence, the simulation on D2 (CNTL-D2) may be viewed as a limited-area mesoscale forecast driven by a hemispheric forecast (from D1).

To investigate how small changes to the initial conditions evolve during this forecast, another simulation of the nested domain is performed that is identical to CNTL-D2 but with perturbed initial conditions (CNTL-D2P). The perturbation to the initial conditions consists of random, Gaussian noise added to the temperature field on D2; the noise has a zero mean, standard deviation 0.2 K, and is independent at each grid point and each grid level. Unlike the perturbations used in ZSR03, which were monochromatic with a wave-

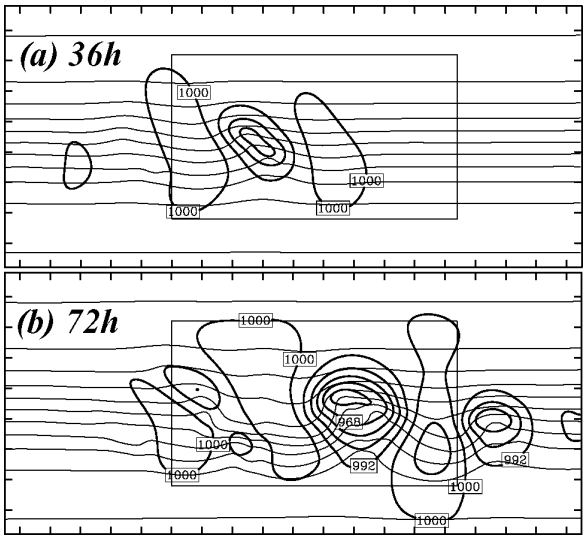

FIG. 2. CNTL-D1 simulated surface potential temperature (thin line, $\Delta = 6$ K) and sea level pressure (thick line, $\Delta = 8$ hPa) valid at (a) 36 and (b) 72 h of the coarse-grid forecast. The gray box denotes the location of the nested domain (D2). The distance between tick marks is 900 km.

length of $O(100$ km), the perturbations used here excite all horizontal scales equally.

The lateral boundary conditions for CNTL-D2P are not perturbed (i.e., they are identical to those of CTRL-D2). As discussed in ZSR02 and elsewhere (e.g., Vukicevic and Errico 1990), fixing the lateral boundary conditions for domains of this size restricts or eliminates growth of perturbations at synoptic scales. Forecast-error growth at synoptic scales is undoubtedly important in practice, but our interest is in growth initiated from smaller scales.

To further investigate the effects of moist convection on mesoscale predictability, several sensitivity experiments reducing the relative humidity to 85%, 70%, 55%, and 40% of that in CNTL [i.e., $(RH)_0 = 85\%$, 70%, 55%, and 40% respectively] are also performed. Reducing the moisture content leads to weaker convective instability at a given time in the simulation. These experiments are called ''EXP85,'' ''EXP70,'' ''EXP55,'' and ''EXP40,'' respectively. Similar to CNTL, each consists of three simulations: a 72-h coarse-domain unperturbed run (D1), a 36-h unperturbed nested run (D2) initialized 36 h after the start of D1, and a 36-h perturbed nested run (D2P).

3. Simulated life cycle of moist baroclinic wave

Figure 2 shows the evolution and the structure of the surface temperature and sea level pressure at different stages of the moist baroclinic wave in CNTL-D1. By 36 h, an incipient cyclone has developed with a minimum sea level pressure of ~975 hPa (Fig. 2a). The simulated baroclinic wave has a zonal wavelength of ~4200 km and moves eastward at a speed of ~21 m s^{-1}. At 72 h, the mature surface cyclone has reached a minimum sea level pressure of ~950 hPa with a ''T bone'' structure and a ''bent back'' warm front (Fig. 2b). The evolution of the surface potential temperature and low-level pressure simulated here is qualitatively similar to the life cycle of a typical extratropical cyclone described by Shapiro and Keyser (1990).

CNTL-D2 is initialized 36 h after the start of CNTL-D1 (Fig. 2a). Over the ensuing 36 h, the simulation CTRL-D2 resembles CTRL-D1, but allows more detailed structure within the baroclinic wave. Figure 3 shows the 6-h accumulated precipitation, as well as sea level pressure and temperature after the first 12- and 24-h integration of CTRL-D2 (corresponding to 48 and

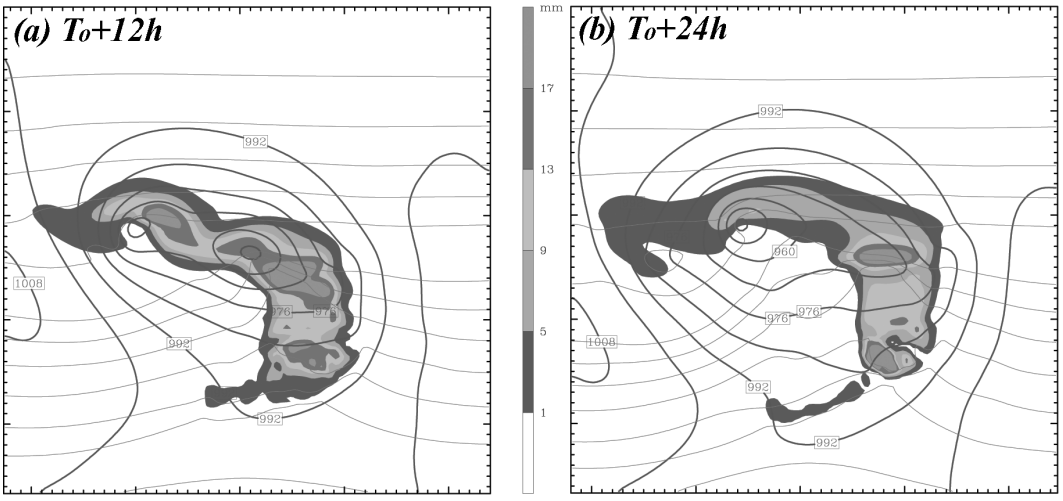

FIG. 3. CNTL-D2 simulated surface potential temperature (thin line, $\Delta = 6$ K), sea level pressure (thick line, $\Delta = 8$ hPa), and 6-h accumulated precipitation (grayscale) valid at (a) 12 and (b) 24 h of the nested domain forecast. The distance between small tick marks is 90 km.

60 h of CTRL-D1, respectively) on a 4200 km × 4200 km window. An elongated warm front is stronger than the cold front, similar to the moist baroclinic waves simulated by Whitaker and Davis (1994) and Fantini (1999). Over the 36-h of nested-grid simulation, the surface cyclone continues to deepen and the total precipitation (6-h accumulations) continues to increase.

In a broad outline, the control simulations reproduce the features found in past primitive equation simulations of dry and moist baroclinic waves (e.g., RSS94; Whitaker and Davis 1994; Shapiro et al. 1999), which features are, in turn, fairly realistic. Hence, we use these simulations as a testbed in which to examine the influence of moist convection on mesoscale predictability.

4. Error growth in simulated moist baroclinic waves

We begin by examining the evolution of the small initial difference between CNTL-D2 and CNTL-D2P. Figure 4 shows the 500-hPa meridional wind difference at 3, 12, 24, and 36 h. By 3 h (Fig. 4a), the wind difference has grown to a maximum of ~0.5 m s^{-1} and is concentrated on the southeast side of the upper trough. At this time, the initial random disturbance added to the temperature field (not shown) has decayed everywhere except for a small region in the southeast quadrant of the upper trough and surface cyclone. Figure 4b shows that over the next 9 h, the differences of the meridional wind remain in a similar location relative to the baroclinic wave, but that the spatial scale and extent increase greatly. The differences have also continued to grow, reaching a maximum of roughly 2.8 m s^{-1} at 12 h. Figures 4c–d show that these trends continue through 36 h as the horizontal scale, spatial extent, and magnitude of the meridional wind are all larger than those at 12 h (Fig. 4b).

Figure 5 shows the 6-h accumulated precipitation difference between CNTL-D2 and CNTL-D2P valid at 12 and 24 h of the nested domain simulation. Maximum differences are roughly 5 and 11 mm at 12 and 24 h, respectively, and their horizontal location corresponds broadly to that of the maximum wind difference at those same times (Figs. 4b,c). Note that differences grow where cumulus parameterization is active, as indicated by the shaded area of significant convective precipitation in Fig. 5). Other regions of significant but nonconvective precipitation (such as that associated with the secondary low at the northeast end of the warm front; Fig. 3) do not support the growing difference. This association of the initial error growth with conditional instability and moist convection was also found in ZSR02 and ZSR03 and again supports the hypothesis that moist convection is responsible for the rapid growth of differences in the simulation.

As in ZSR03, we define the difference total energy (DTE) as

$$\mathrm{DTE} = \frac{1}{2}(U'^2_{ijk} + V'^2_{ijk} + \kappa T'^2_{ijk}), \qquad (1)$$

where U', V', and T' are the difference wind components and difference temperature between two simulations, $\kappa = C_p/T_r$ (the reference temperature $T_r = 287$/K), and i, j, and k run over x, y, and σ grid points over one horizontal wavelength of the baroclinic waves (a box of 4200 km × 4200 km used for Figs. 4–5). A power-spectrum analysis of DTE is shown in Fig. 6. At 0 h, the spectral density of the initial random perturbation (which is white noise added only to the temperature field) is proportional to the (global) horizontal wavenumber [$\kappa = (k^2 + l^2)^{0.5}$, where k and l are the horizontal wavenumber in the x and y directions].[1] Over the first 3 h, the smaller-scale (<120 km) components of the DTE spectrum decrease dramatically owing largely to model diffusion. Similar behavior in quasigeostrophic models has been discussed in Wirth and Ghil (2000) and Snyder et al. (2003). Consistent with the visual impression from the error field shown in Fig. 4, DTE grows steadily at larger wavelengths over the entire forecast period to 36 h. Over the same interval, the peak of the spectrum gradually migrates with time to larger scales (700 ~ 1000 km after 36 h) as both the scale of variation of the differences and their areal extent increase (Figs. 4c,d). The differences grow and spread upscale in the present idealized baroclinic wave in a manner that is qualitatively similar to that in the 30-km simulations of ZSR03 (see their Fig. 3).

The comparison between the current idealized study and ZSR03 is also of interest. The initial, white-noise perturbations employed here differ from those used in ZSR03. To make direct and quantitative comparison of the current study to ZSR03, we have performed an additional experiment (''CNTL-4DX'') by adding the same monochromatic wave perturbation used in ZSR03 [refer to Eq. (1) of ZSR03, p. 1175] to D2 at 36 h.

After 36 h, the scale and magnitude of the difference between CNTL-D2 and CNTL-4DX are very similar to those between CNTL-D2 and CNTL-D2P (not shown). The location of the difference within the baroclinic wave is also comparable to that shown in Fig. 4d. Thus, the response is not particularly sensitive to the details of the initial differences, much as was found by ZSR02 for the surprise snowstorm.

In terms of DTE, the amplification over 36 h of the difference between CNTL-D2 and CNTL-4DX (not shown) is ~¼ of that between CNTL-30km and PERT-30km in ZSR03. Consistent with the DTE amplifications, maximum differences in U, V, and T at 36 h are roughly a factor of two smaller than those in ZSR03.

[1] Note that the curves in the figure show the perturbation energy at each wavelength [corresponding to $\kappa = (k^2 + l^2)^{1/2}$], hence the spectral density for two-dimensional field of white noise is inversely proportional to the wavelength (rather than constant across all wavelengths).

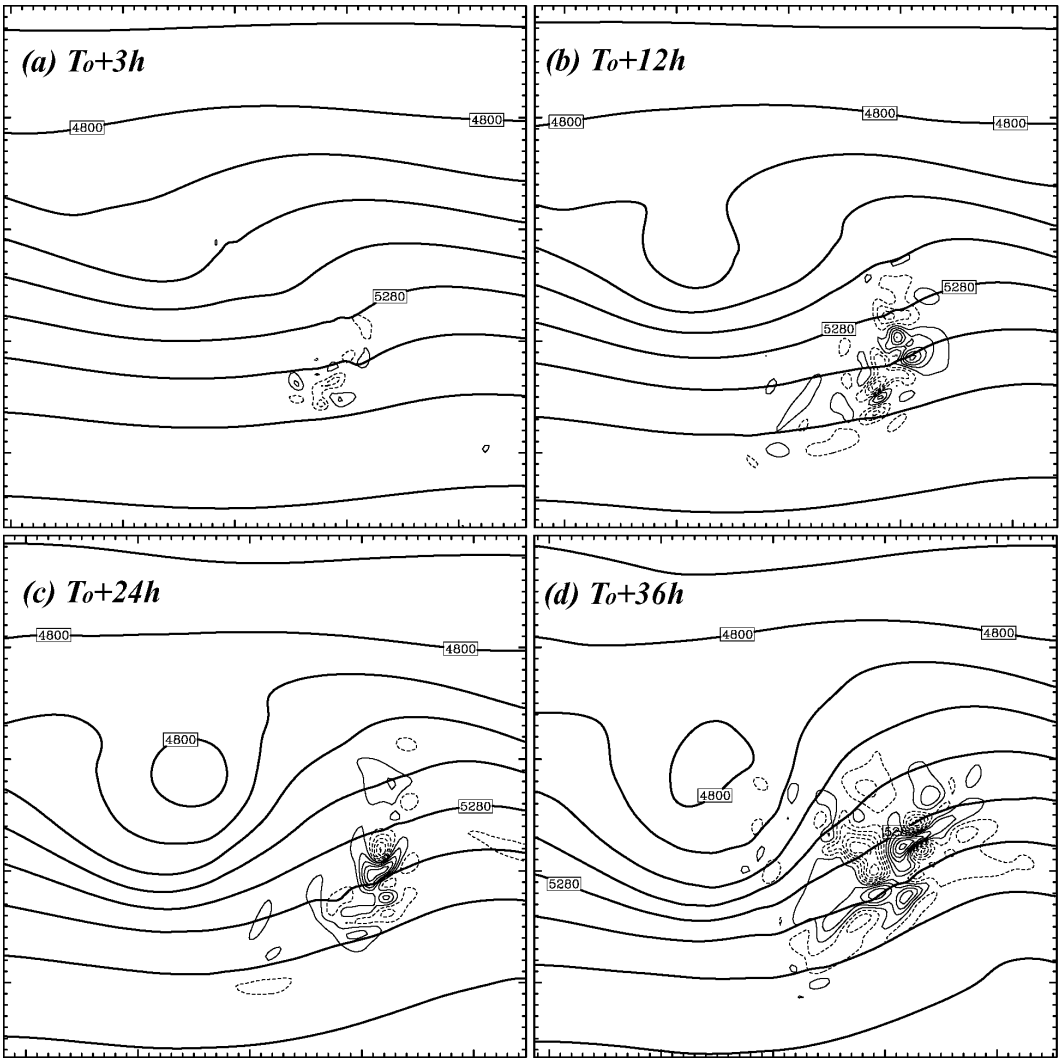

FIG. 4. The 500-hPa meridional wind difference (thin lines; negative, dashed) between CNTL-D2 and CNTL-D2P valid at (a) 3, (b) 12, (c) 24, and (d) 36 h of the nested domain simulation. Contour intervals are 0.2 m s^{-1} for (a), 0.5 m s^{-1} for (b), and 1.0 m s^{-1} for (c) and (d), respectively. The 500-hPa geopotential height (every 120 dam) in CNTL-D2 is also shown in thick lines. The distance between small tick marks is 90 km. The display window moves east.

The differences in error growth between the current study and ZSR03 could be associated with detailed differences in the simulations such as the intensity and areal coverage of the CAPE or the amplitude and growth rate of the parent baroclinic waves. The relative lack of mesoscale error in the current study also suggests the importance of other factors, not included in the idealized moist baroclinic wave, in determining the error growth in the surprise snow storm.

The present results are obtained in a model in which moist convection is parameterized. As in ZSR03, the difference growth is not sensitive to the selection and formulation of cumulus parameterization schemes. For the 30-km resolution, simulations identical to CNTL-D2 and CNTL-D2P but with only explicit microphysics (no cumulus parameterization) yield similar error growth characteristics.

5. Effects of initial moisture distribution

To further test the impacts of moist convection on mesoscale predictability, we examine the error growth in the sensitivity experiment EXP70 in which the initial relative humidity is reduced to 70% of that in CNTL. EXP70-D2P uses exactly the same initial perturbations as in CNTL-D2P. Figure 7 shows the 500-hPa meridional wind difference between EXP70-D2 and EXP70-D2P at 12 and 24 h, respectively, while Fig. 8 shows that the 6-h accumulated precipitation difference valid at the same times. As in the CNTL experiment, there

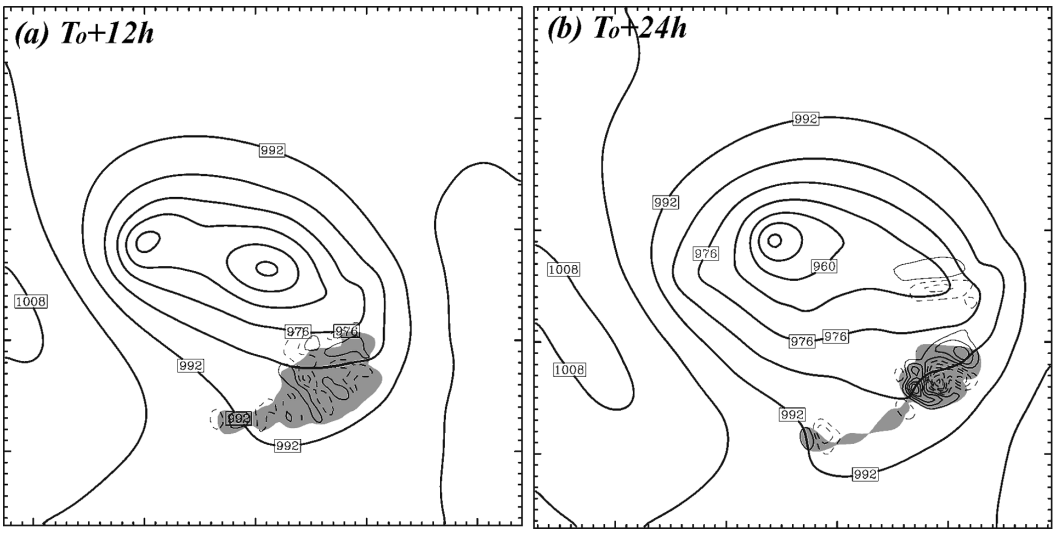

FIG. 5. The 6-h accumulated precipitation difference (thin lines; negative, dashed; contour interval 2 mm) between CNTL-D2 and CNTL-D2P valid at (a) 12 and (b) 24 h of the nested domain simulation. The sea level pressure (every 8 hPa) simulated by CNTL-D2 is also shown in thick lines. Areas with the 6-h accumulated convective precipitation greater than 1 mm in CNTL-D2 are shaded. The distance between small tick marks is 90 km. The display windows are the same as in Fig. 4.

is a rapid initial decay of the random noise everywhere except in the southeast quadrant of the surface cyclone; the initial error then spreads over a larger area and increases in horizontal scale. However, with a much reduced initial moisture content, and thus much weaker convective instability over this area, the growth of the error in EXP70 is much weaker than that of CNTL. Besides a smaller areal coverage, the maximum 500-hPa meridional wind difference in EXP70 is only ~1.3 m s^{-1} at 12 h and ~2.5 m s^{-1} at 24 h (Fig. 7), which are less than half of those found in CNTL. The 6-h accumulated precipitation difference (Fig. 8), which occurs primarily in the region of parameterized moist convection, is also greatly reduced over the same period (cf. Fig. 8 with Fig. 5).

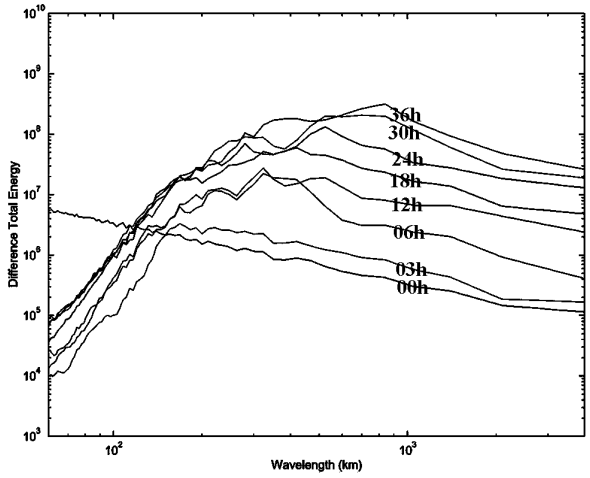

FIG. 6. Power spectra of the DTE (m^2 s^{-2}) between CNTL-D2 and CNTL-D2P plotted every 6 h from 0 h as well as at 3 h.

Power spectra of DTE for several times from EXP70 are shown in Fig. 9. Much as in CNTL, the DTE at smaller scales decreases rapidly over the first 3 to 6 h. Because of weaker convective activity and smaller areal coverage of the convection, however, the growth in the convective area becomes evident in DTE, which is a domain-integrated quantity, only after the first 12 h. (The interplay between general decay and local growth of differences is discussed further below.) DTE grows steadily at all wavelengths over the subsequent forecast period out to 36 h. Because DTE decays over a larger initial period in EXP70, it remains smaller than in CNTL at all wavelengths and does not saturate at any wavelength, even after 36 h. The shift of the peak of the spectrum toward larger scales is also less evident than in CNTL.

Sensitivity experiments EXP85, EXP55, and EXP40, in which the initial relative humidity was reduced to 85%, 55%, and 40% of that in CNTL, respectively, were also performed with the same initial difference as in CNTL in the nested domain. The impacts of moist convection on mesoscale predictability is summarized by the DTE time series shown in Fig. 10, which show decreasing error growth with decreasing humidity. Figure 10a shows there is a sharp ''decrease'' of DTE in all the experiments (including CNTL) over the first 3 h. This decrease can be understood as a consequence of the fact that the initial error decays through diffusion or geostrophic adjustment over vast portions of the averaging domain (the wavelength of the baroclinic wave) and grows only in a limited area near the surface low

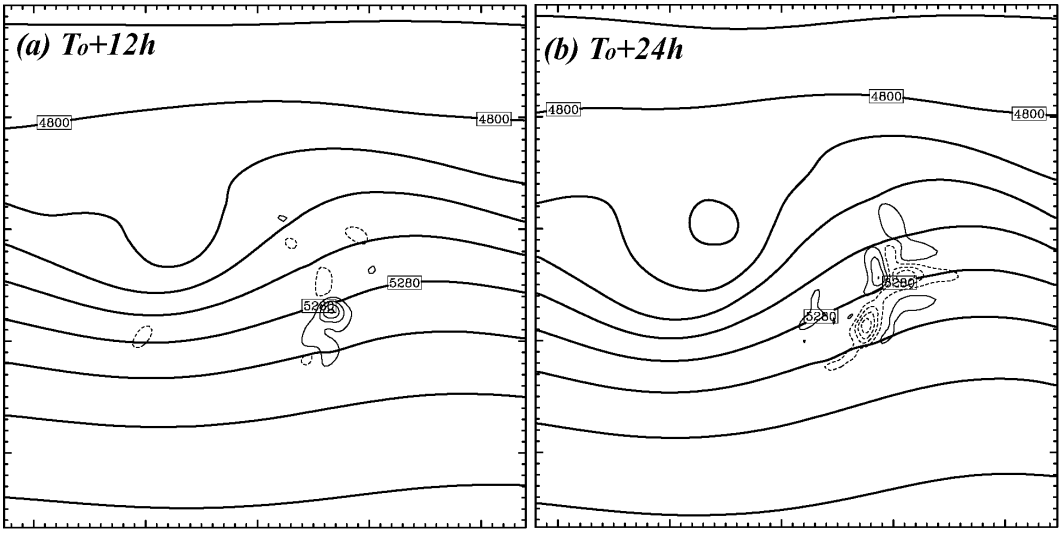

FIG. 7. As in Fig. 4, except for the 500-hPa meridional wind difference between EXP70-D2 and EXP70-D2P valid at (a) 12 and (b) 24 h of the nested domain simulation. Contour intervals are 0.2 m s^{-1} for (a) and 0.5 m s^{-1} for (b).

where there is moist convection. Figure 10b shows that computing DTE over a smaller averaging domain (1500 km by 1500 km) surrounding the convective activity indicates strong error growth in CNTL even over the first 3 h and ''less'' decrease in the other experiments.

In spite of the strong variations of the growth rates in the different experiments over different periods, by and large, Fig. 10 indicates that larger initial relative humidity corresponds to more rapid error growth. Since the simulations with larger relative humidity exhibit greater conditional instability and stronger parameterized convection, the relation between initial humidity and error growth also supports our assertion that the moist convection controls the initial phase of the error growth. Moreover, with a maximum initial RH of only 40%, EXP40 exhibits little precipitation (either explicit or convective) and is dominated by dry dynamics. There is hardly any error growth in EXP40 over the entire 36-h forecast period. Indeed, consistent with the findings of ZSR02 and ZSR03, the evolution of DTE in EXP40 is similar to a ''fake dry'' version of the control experiment (not shown) in which no latent heating/cooling from moist processes was allowed.

The aforementioned experiments and those from

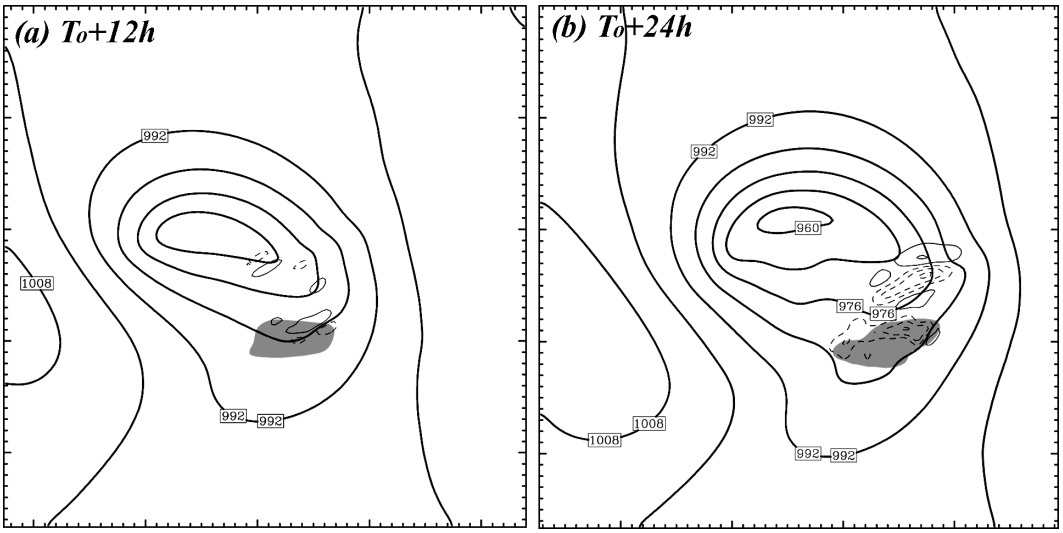

FIG. 8. The 6-h accumulated precipitation difference (thin lines; negative, dashed; contour interval 0.5 mm) between EXP70-D2 and EXP70-D2P valid at (a) 12 and (b) 24 h of the nested domain simulation. The sea level pressure (every 8 hPa) simulated by EXP70-D2 is also shown in thick lines. Areas with the 6-h accumulated convective precipitation greater than 1 mm in EXP70-D2 are shaded. The distance between small tick marks is 90 km. The display windows are the same as in Fig. 4.

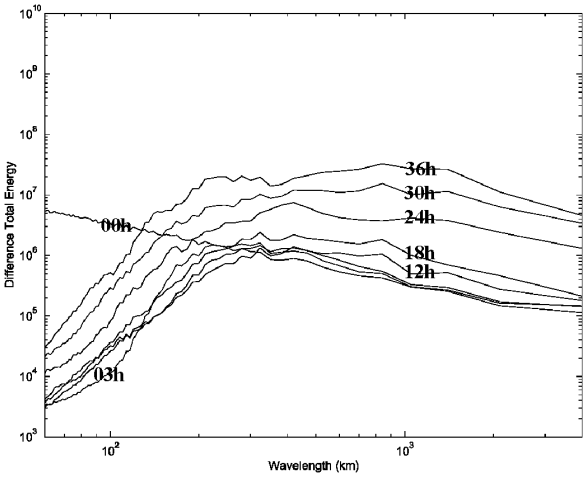

FIG. 9. Power spectra of the DTE ($m^2\ s^{-2}$) between EXP70-D2 and EXP70-D2P plotted every 6 h from 0 h as well as at 3 h.

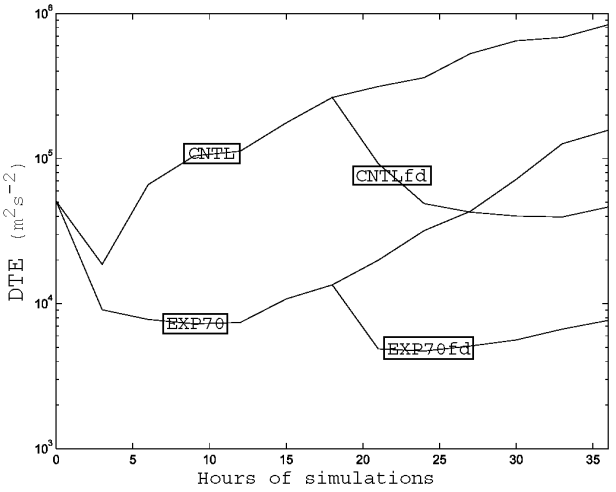

FIG. 11. Evolution of DTE ($m^2\ s^{-2}$) integrated over a horizontal wavelength of the baroclinic wave in experiments with and without latent heating/cooling for experiments CNTL and EXP70. In CNTLfd and EXP70, latent heating/cooling is turned off after 18 h of the nested domain integration.

ZSR03 strongly suggest that moist convection or its parameterization is essential in organizing and amplifying small-scale, small-amplitude disturbances over the first 3–6 h of the simulations. After the initial period of decay of DTE, however, Fig. 10 indicates similar rates of amplification in all but EXP40. One may thus ask whether convection (or moist processes) is necessary to sustain the error growth after the difference energy has already grown and spread to larger scales. Two additional experiments, namely, ''CNTLfd'' and ''EXP70fd,'' are performed in a manner similar to CNTL and EXP70 except that, after 18 h of the nested domain integration, latent heating/cooling from moist processes is turned off in both the perturbed and unperturbed runs. The subsequent DTE evolutions from these two fake dry experiments are plotted in Fig. 11, from which we can see that DTE drops quickly and reduces to less than an order of magnitude of their moist counterparts after another 18 h of fake dry integration. The results from these two fake dry experiments further demonstrate fundamental differences exist between dry and moist dynamics in terms of mesoscale predictability.

6. Summary and discussion

The present work represents a step on the path toward understanding how forecast errors grow. The vast majority of work on this topic is directed toward the modalities of error growth on the synoptic scale where effects of moisture might plausibly be neglected (see ZSR03 for a review). Using a forecast model that is representative of those currently used for mesoscale numerical weather prediction (MM5), including the standard ''physics,'' we have examined how errors grow as a function of the moist instability within the context of

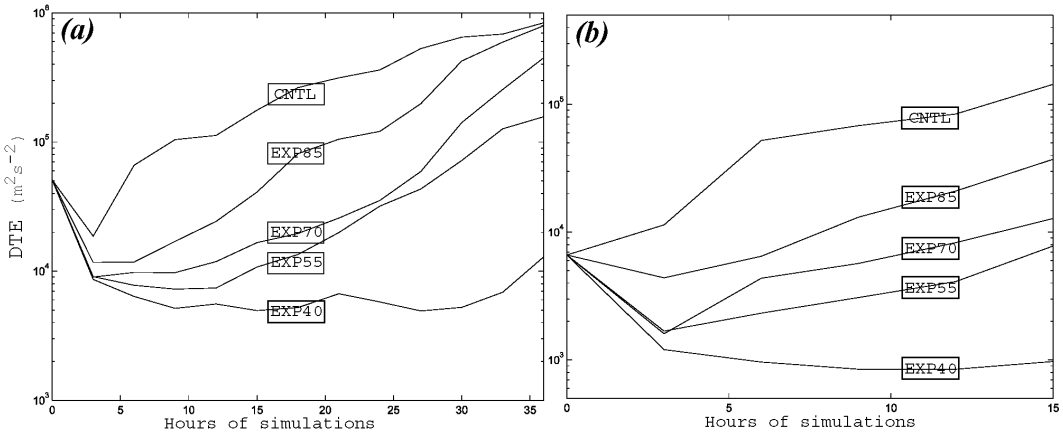

FIG. 10. (a) Evolution of DTE ($m^2\ s^{-2}$) integrated over a horizontal wavelength of the baroclinic wave in experiments with different initial basic-state RH, that is, CNTL, EXP85, EXP70, EXP55, and EXP40. (b) As in (a), but the DTE is integrated over a smaller (1500 km × 1500 km) domain surrounding the convective area for 15 h.

a simple, but realistic, synoptic-scale development represented by the downstream development of a baroclinic wave. Our results indicate that, without the effects of moisture, there is little error growth in the short-term (0–36 h) difference between two simulations (starting from random noise), even though the basic jet used here produces a rapidly growing synoptic-scale disturbance. This result generalizes that of ZSR03 obtained from a single case study.

There are also noticeable differences between the current idealized study and ZSR03. Direct comparisons show that the 36-h amplification of errors in the present (CNTL) simulations is about half of that found in ZSR03 at the same resolution. The reasons for these differences are not certain at this time, but differences in the amplitude of the parent baroclinic wave, the details of its development, or lack of a large area of convective instability (which is associated with the warm Gulf Stream in ZSR03), are possible contributors.

In a future study we intend to employ an analogous high-resolution explicit-convection inner domain (i.e., a D3) in the context of the present idealized simulations. From these latter simulations, or possibly further simplifications thereof, we hope to discover the mechanisms for error growth and if and how they are related to those mechanisms discussed from either statistical predictability theory (e.g. Lesieur 1997, chapter XI) or from dynamical systems of the type discussed in Bohr et al. (1998, chapter VI).

Acknowledgments. We are grateful to Chris Davis for providing the codes for PV inversion, and to Rebecca Morss and two anonymous reviewers for providing thorough reviews of earlier versions of the manuscript. This research was supported at NCAR by the U.S. Weather Research Program. ZMT was also supported by Natural Science Foundation of China; FZ was also supported by NSF Grant ATM-0205599 and by the Young Investigator Program of the Department of Navy, Office of Navy Research. Any opinions, findings, and conclusions or recommendations expressed in this paper are those of the authors and do not necessarily reflect the views of the Office of Navy Research.

APPENDIX

Initial Moisture Field

The initial, x-independent relative humidity is given by

$$\mathrm{RH}(y, z) = \begin{cases} \mathrm{RH}_0\left[1 - 0.9\left(\dfrac{z}{z_{\mathrm{rh}}}\right)^{\delta} R(y)\right] & \text{when } z < z_{\mathrm{rh}}; \\ \mathrm{RH}_1 R(y) & \text{when } z \geq z_{\mathrm{rh}}; \end{cases} \tag{A1}$$

$$R(y) = \begin{cases} R_1, & y < y_1; \\ R_1 + \dfrac{y - y_1}{y - y_2}(R_2 - R_1), & y_1 \leq y < y_2; \\ R_2, & y \geq y_2; \end{cases} \tag{A2}$$

where $R_1 = 0.5$, $R_2 = 1.0$, $y_1 = 0.4y_c$, $y_2 = 0.8y_c$, $y_c = 4050$ km, $\mathrm{RH}_1 = 9.0$, $z_{\mathrm{rh}} = 9000$ m, and $\delta = 2.0$.

The various experiments use the following values of RH_0:

CNTL: $\mathrm{RH}_0 = 100.0$,

EXP85: $\mathrm{RH}_0 = 85.0$,

EXP70: $\mathrm{RH}_0 = 70.0$,

EXP55: $\mathrm{RH}_0 = 55.0$, and

EXP40: $\mathrm{RH}_0 = 40.0$.

REFERENCES

Bohr, T., M. H. Jensen, G. Paladin, and A. Vulpiani, 1998: *Dynamical Systems Approach to Turbulence.* Cambridge University Press, 350 pp.

Davis, C. A., and K. A. Emanuel, 1991: Potential vorticity diagnosis of cyclogenesis. *Mon. Wea. Rev.,* **119,** 1929–1952.

Dudhia, J., 1993: A nonhydrostatic version of the Penn State/NCAR Mesoscale Model: Validation tests and simulation of an Atlantic cyclone and cold front. *Mon. Wea. Rev.,* **121,** 1493–1513.

Ehrendorfer, M., R. M. Errico, and K. D. Raeder, 1999: Singular-vector perturbation growth in a primitive equation model with moist physics. *J. Atmos. Sci.,* **56,** 1627–1648.

Fantini, M., 1999: Evolution of moist-baroclinic normal modes in the nonlinear regime. *J. Atmos. Sci.,* **56,** 3161–3166.

Grell, G. A., 1993: Prognostic evaluation of assumptions used by cumulus parameterizations. *Mon. Wea. Rev.,* **121,** 5–31.

Hakim, G. J., 2000: Role of nonmodal growth and nonlinearity in cyclogenesis initial-value problems. *J. Atmos. Sci.,* **57,** 2951–2967.

Hong, S.-Y., and H.-L. Pan, 1996: Nonlocal boundary layer vertical diffusion in a medium-range forecast model. *Mon. Wea. Rev.,* **124,** 2322–2339.

Langland, R. H., M. A. Shapiro, and R. Gelaro, 2002: Initial condition sensitivity and error growth in forecasts of the 25 January 2000 east coast snowstorm. *Mon. Wea. Rev.,* **130,** 957–974.

Lesieur, M., 1997: *Turbulence in Fluids.* 3d ed. Martinus Nijhoff, 515 pp.

Lorenz, E. N., 1969: The predictability of a flow which possesses many scales of motion. *Tellus,* **21,** 289–307.

Reisner, J., R. J. Rasmussen, and R. T. Bruintjes, 1998: Explicit forecasting of supercooled liquid water in winter storms using the MM5 Mesoscale Model. *Quart. J. Roy. Meteor. Soc.,* **124B,** 1071–1107.

Rotunno, R., and J.-W. Bao, 1996: A case study of cyclogenesis using a model hierarchy. *Mon. Wea. Rev.,* **124,** 1051–1066.

——, W. C. Skamarock, and C. Snyder, 1994: An analysis of frontogenesis in numerical simulations of baroclinic waves. *J. Atmos. Sci.,* **51,** 3373–3398.

Shapiro, M. A., and D. Keyser, 1990: Fronts, jet streams, and the tropopause. *Extratropical Cyclones: The Erik Palmen Memorial Volume,* C. W. Newton and E. O. Holopainen, Eds., Amer. Meteor. Soc., 167–191.

——, and Coauthors, 1999: A planetary-scale to mesoscale perspective of the life cycles of extratropical cyclones: The bridge be-

tween theory and observations. *The Life Cycles of Extratropical Cyclones,* M. A. Shapiro and S. Gronas, Eds., Amer. Meteor. Soc., 1228–1251.

Snyder, C., T. M. Hamill, and S. Trier, 2003: Linear evolution of forecast error covariances in a quasigeostrophic model. *Mon. Wea. Rev.,* **131,** 189–205.

Vukicevic, T., and R. M. Errico, 1990: The influence of artificial and physical factors upon predictability estimates using a complex limited-area model. *Mon. Wea. Rev.,* **118,** 1460–1482.

Whitaker, J. S., and C. A. Davis, 1994: Cyclogenesis in a saturated environment. *J. Atmos. Sci.,* **51,** 889–907.

Wirth, A., and M. Ghil, 2000: Error evolution in the dynamics of an ocean general circulation model. *Dyn. Atmos. Oceans,* **32,** 419–431.

Zhang, F., 2004: Generation of mesoscale gravity waves in upper-tropospheric jet–front systems. *J. Atmos. Sci.,* **61,** 440–457.

——, C. Snyder, and R. Rotunno, 2002: Mesoscale predictability of the ''surprise'' snowstorm of 24–25 January 2000. *Mon. Wea. Rev.,* **130,** 1617–1632.

——, ——, and ——, 2003: Effects of moist convection on mesoscale predictability. *J. Atmos. Sci.,* **60,** 1173–1185.

CORRIGENDUM

ZHE-MIN TAN

Department of Atmospheric Sciences, Nanjing University, Nanjing, China

FUQING ZHANG

Department of Atmospheric Sciences, Texas A&M University, College Station, Texas

RICHARD ROTUNNO AND CHRIS SNYDER

National Center for Atmospheric Research, Boulder, Colorado

The appendix of Tan et al. (2004) had typographic errors in (A1) and (A2) and in several of the parameters in these equations. The correct versions of (A1), (A2), and the parameters, respectively, are

$$\mathrm{RH}(y, z) = \mathrm{RH}_0 R(y) \begin{cases} 1 - 0.9\left(\dfrac{z}{z_{rh}}\right)^{\delta} & z < z_{rh}, \\ 0.1 & z \geq z_{rh}, \end{cases} \tag{A1}$$

$$R(y) = \begin{cases} R_1, & y \leq y_1 \\ R_1 + \dfrac{y - y_1}{y_2 - y_1}(R_2 - R_1), & y_1 < y < y_2 \\ R_2, & y \geq y_2 \end{cases}, \tag{A2}$$

where $R_1 = 0.5$, $R_2 = 1.0$, $y_1 = 0.4y_c$, $y_2 = 0.8y_c$, $y_c = 4005$ km, $z_{rh} = 8000$ m, and $\delta = 1.25$. For the control run (CNTL), $\mathrm{RH}_0 = 92.0$ (not $\mathrm{RH}_0 = 100.0$). All calculations reported in Tan et al. (2004) used the correct formulations given here.

REFERENCES

Tan, Z.-M., F. Zhang, R. Rotunno, and C. Snyder, 2004: Mesoscale predictability of moist baroclinic waves: Experiments with parameterized convection. *J. Atmos. Sci.,* **61,** 1794–1804.

Corresponding author address: Fuqing Zhang, Department of Atmospheric Sciences, Texas A&M University, College Station, TX 77843-3150.
E-mail: fzhang@tamu.edu

DOI: 10.1175/2007JAS2715.1